Anion	SCN^-	$PO_2F_2^-$	I^-	SO_3F^-	BF_4^-	ReO_4^-	TcO_4^-	PF_6^-	ClO_4^-	Br^-	CN^-	NO_3^-	N_3^-
Anion volume (A^3)	71 ± 3	90 ± 6	72 ± 16	88 ± 4	73 ± 9	86 ± 13	93 ± 2	109 ± 8	82 ± 13	56 ± 14	50 ± 6	64 ± 11	58 ± 14
IC_{50} vs. $^{99m}TcO_4^-$ uptake, 3E.Δ-NIS cells	8.3 (K)	3.9 (NH_4)	2.7 (K)	0.56 (K)	0.29 (K)	0.15 (K)	0.07 (NH_4)	0.021 (K)	N/D	N/D	N/D	N/D	N/D
IC_{50} vs. $^{99m}TcO_4^-$ uptake, HCT116-C19 cells	8.5 (K)	6.9 (NH_4)	4.7 (Na)	0.55 (K)	4.5 (Na)	N/D	N/D	0.026 (K)	N/D	N/D	N/D	755 (Na)	N/D
IC_{50} vs. $^{127}I^-$ uptake, FRTL5 cells (*1*)	12 (Na)	N/D	N/D	N/D	1.2 (Na)	N/D	N/D	0.015 (K)	0.1 (Na)	3300 (Na)	1900 (K)	800 (Na)	2200 (Na)
IC_{50} vs. $^{125}I^-$ uptake, FRTL5 cells (*1*)	14 (Na)	N/D	N/D	N/D	0.75 (Na)	N/D	N/D	0.009 (K)	0.14 (Na)	1400 (Na)	1700 (K)	250 (Na)	1200 (Na)
IC_{50} vs. $^{125}I^-$ uptake, CHO-hNIS cells (*2*)	19.3	N/D	33.9 (Na)	N/D	N/D	N/D	N/D	N/D	1.27	N/D	N/D	297	N/D
IC_{50} vs. $^{125}I^-$ uptake, FRTL5 cells (*3*)	N/D	N/D	N/D	N/D	0.7 (K)	N/D	N/D	N/D	0.4 (K)	N/D	N/D	N/D	N/D
IC_{50} vs. ^{18}F-BF_4^- uptake, HCT116-C19 cells (*4*)	N/D	N/D	N/D	N/D	1.6 (Na)	N/D	N/D	N/D	N/D	N/D	N/D	N/D	N/D
IC_{50} vs. $^{99m}TcO_4^-$ uptake, HCT116-C19 cells (*4*)	N/D	N/D	N/D	N/D	0.74 (Na)	N/D	N/D	N/D	N/D	N/D	N/D	N/D	N/D
IC_{50} vs. ^{18}F-BF_4^- uptake, HCT116-C19 cells (*5*)	N/D	N/D	N/D	N/D	4.8 (Na)	N/D	N/D	N/D	N/D	N/D	N/D	N/D	N/D
IC_{50} vs. ^{18}F-SO_3F^- uptake, HCT116-C19 cells	N/D	N/D	N/D	1.6 (K)	N/D	N/D	N/D	N/D	N/D	N/D	N/D	N/D	N/D

Supplemental Table 1. IC_{50} values (μM) against anion transport in various cell lines and corresponding volumes (*6*) for univalent anions. Counter-cation is given in brackets after IC_{50} value (if known). N/D = not determined.

Entry	**Base**	**Precursor (mg)**	**Temp. (°C)**	**Time (min)**	**Radiochemical yield (%)***
1	$KHCO_3$	5	80	15	38
2	$KHCO_3$	5	30	15	7
3	K_2CO_3	5	80	15	50
4	K_2CO_3	0.5	80	15	14

5	K_2CO_3	5	80	10	65
6	K_2CO_3	5	80	20	38
7	K_2CO_3	5	80	5	25

Supplemental Table 2. Radiochemical yield values for reaction of ^{18}F-KF with SO_3-pyridine under varying conditions, as determined by ion chromatography (details in main manuscript) *Pre-purification yield in crude reaction mixture

	0.9% NaCl @ 25°C	Human serum @ 37°C	HCl/glycine buffer (pH 3.0) @ 37°C
0 h	99	99	95
1 h	ND	98	95
2 h	ND	98	95
3 h	ND	98	95
4 h	99	98	94

Supplemental Table 3. Radiochemical purity (%) of ^{18}F-SO_3F^- incubated in saline, serum or acidic buffer over a 4 hour time period, as determined by ion chromatography (0.9% NaCl) and TLC (human serum and HCl/Glycine buffer). Details of analytical methods are given in main manuscript.

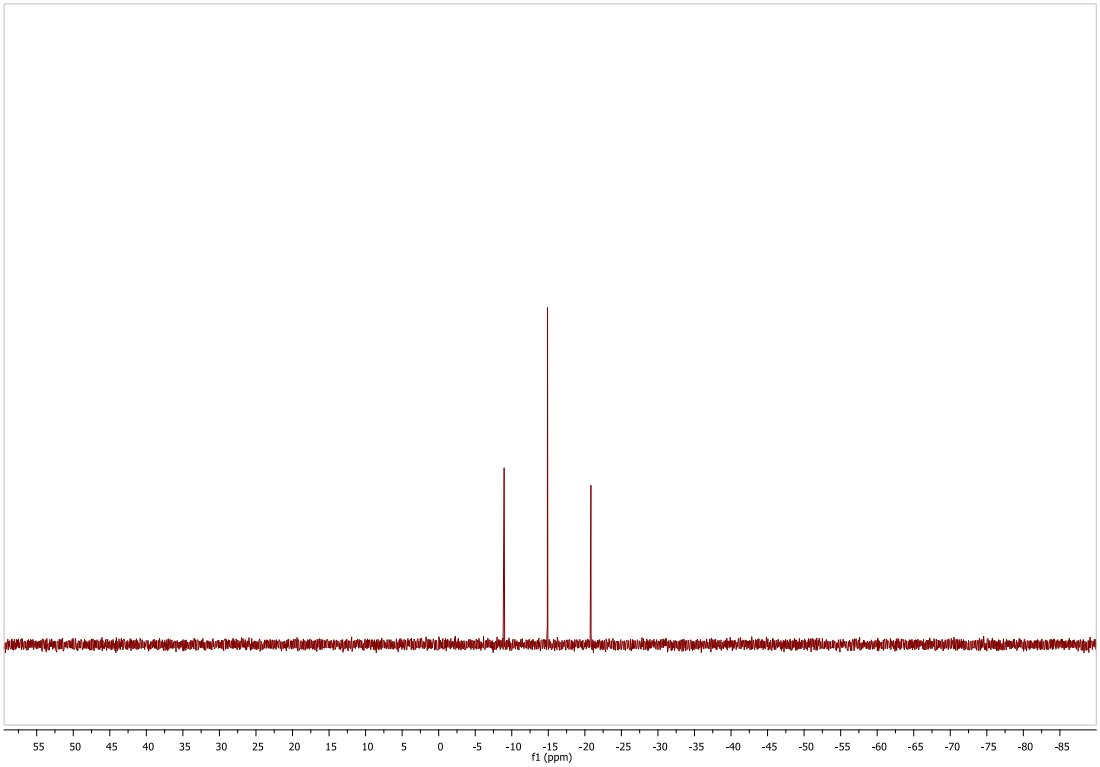

Supplemental Figure 1. ^{31}P NMR spectrum of $NH_4PO_2F_2$ showing a triplet at δ 14.89 (J = 962.1 MHz) owing to coupling to two ^{19}F nuclei. Data collected using Bruker Ultrashield 400WB PLUS 9.4 T spectrometer operating at a frequency of 161.976 MHz. The compound was analyzed as a solution (5 mg/mL) in D_2O. Data were analyzed using MestReNova LITE (v5.2.5-5780).

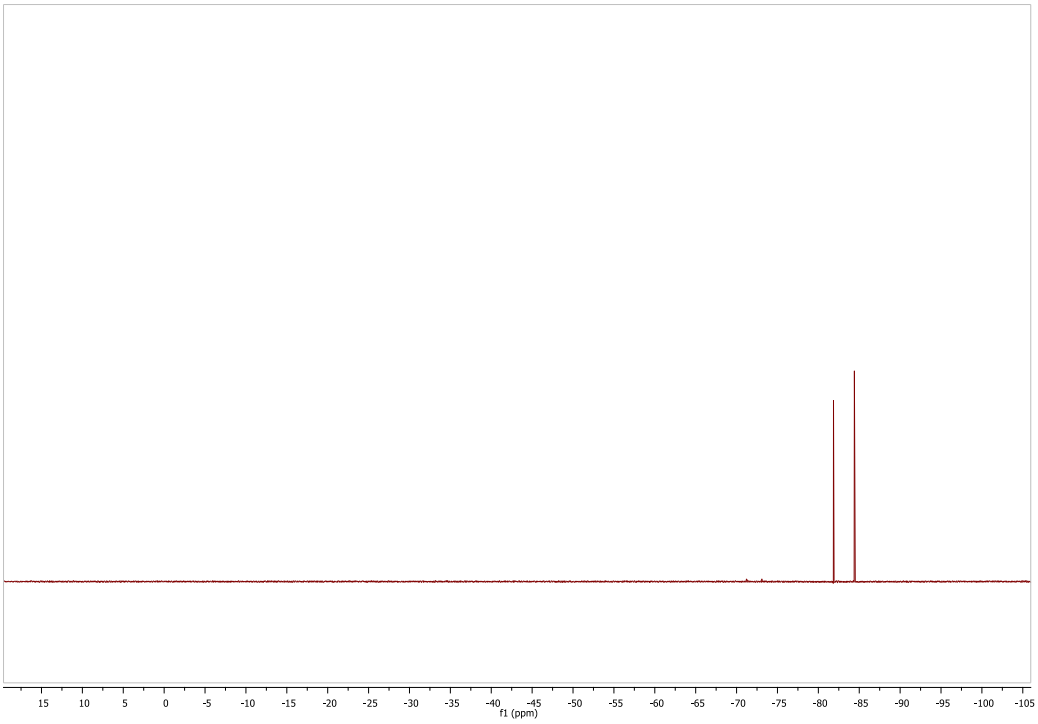

Supplemental Figure 2. ^{19}F NMR spectrum of $NH_4PO_2F_2$ showing a doublet at δ -83.14 (J = 971.4 MHz) owing to coupling to a single ^{31}P nucleus. Data collected using Bruker Ultrashield 400WB PLUS 9.4 T spectrometer operating at a frequency of 376.461 MHz respectively. The compound was analyzed as a solution (5 mg/mL) in D_2O. Data were analyzed using MestReNova LITE (v5.2.5-5780).

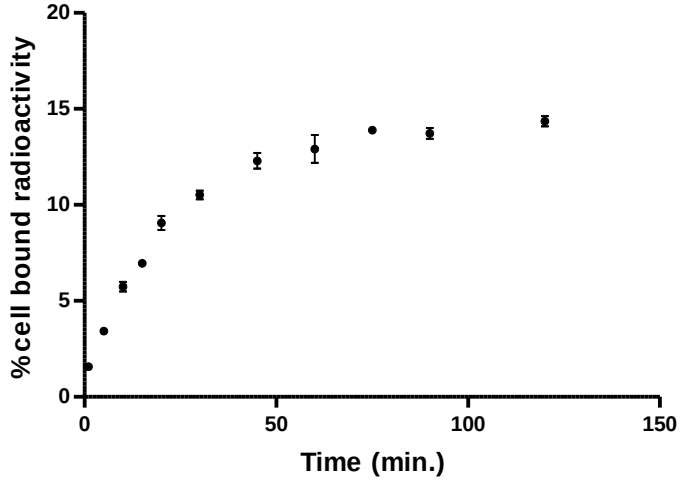

Supplemental Figure 3. Uptake of ^{18}F-SO_3F^- in HCT116-C19 cells over a 2 h time period, assessed as % radioactivity bound to cells. Error bars represent 1 S.D.

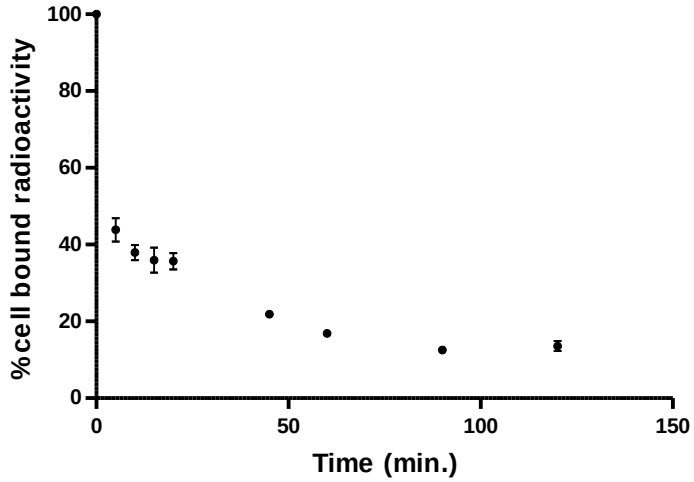

Supplemental Figure 4. Efflux of $^{18}F\text{-}SO_3F^-$ from HCT116-C19 cells over a 2 h time period, displayed as % remaining cell bound radioactivity. At t = 0 min it was assumed that all remaining activity was cell bound following the washing protocol and that this represented maximal cell bound activity (100%). Error bars represent 1 S.D.

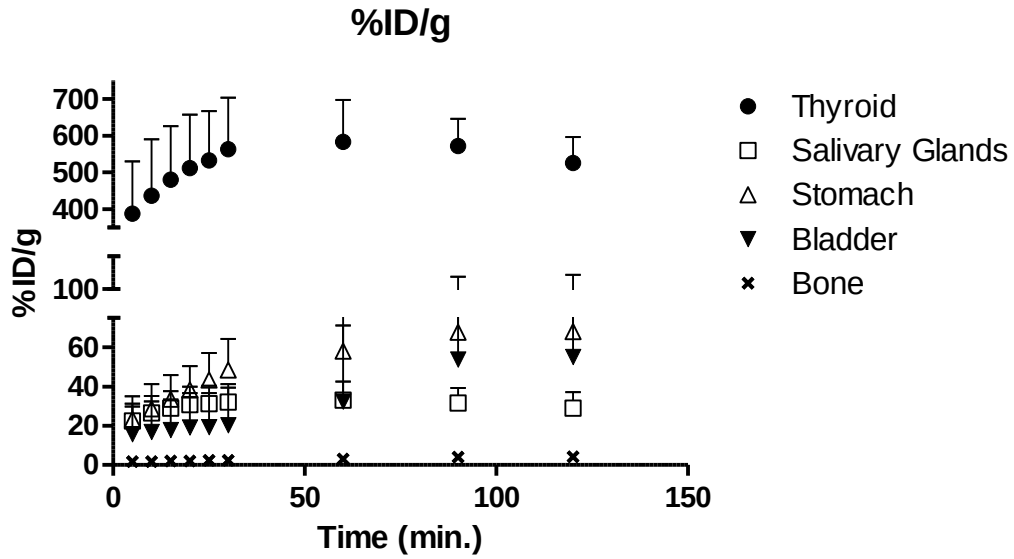

Supplemental Figure 5. Time-activity curve displaying %ID/g values calculated from PET/CT images for thyroid, salivary glands, stomach, and bladder over a 2 h time period in BALB/c mice without $NaClO_4$ inhibition (n = 3).

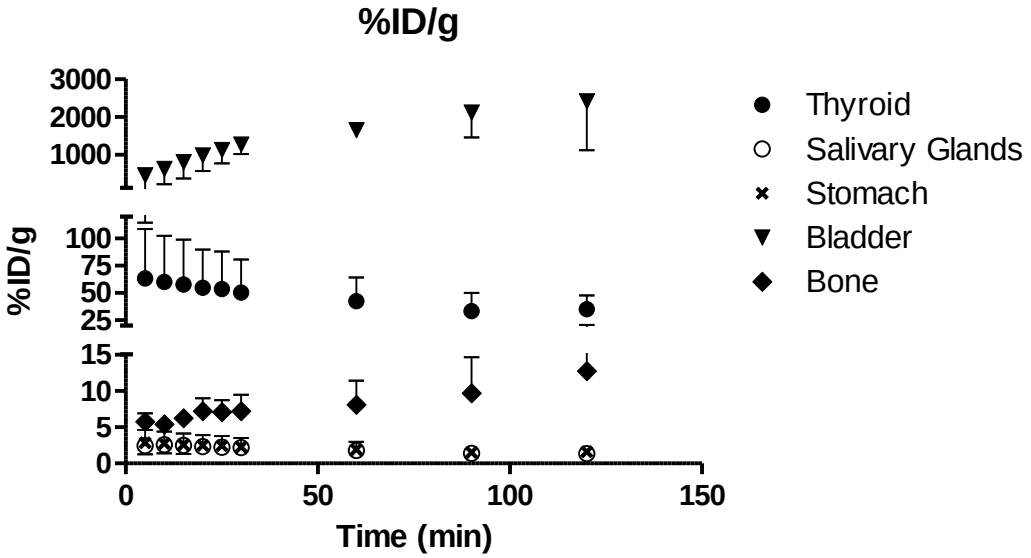

Supplemental Figure 6. Time-activity curve displaying %ID/g values calculated from PET/CT images for thyroid, salivary glands, stomach, and bladder over a 2 h time period in BALB/c mice with $NaClO_4$ inhibition (n = 3).

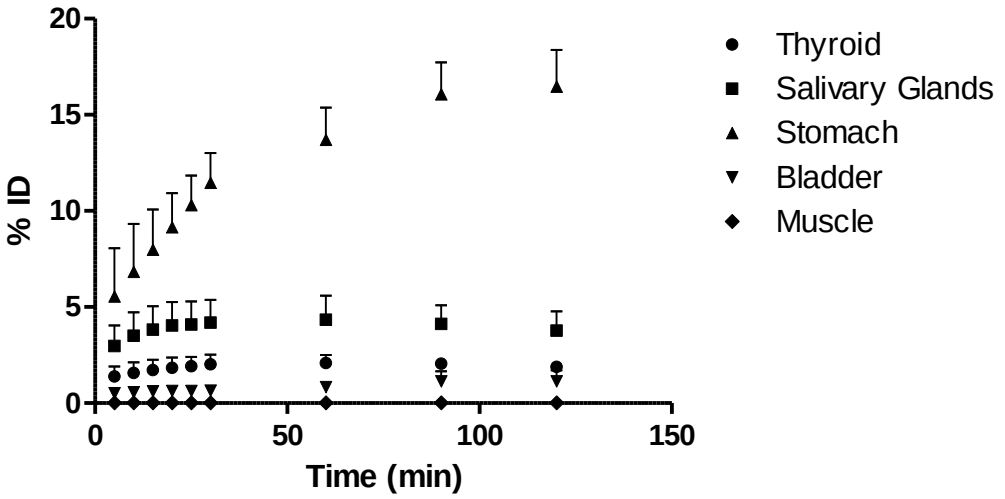

Supplemental Figure 7. Time-activity curve displaying %ID values calculated from PET/CT images for thyroid, salivary glands, stomach, bladder, and muscle over a 2 h time period in BALB/c mice without $NaClO_4$ inhibition (n = 3)

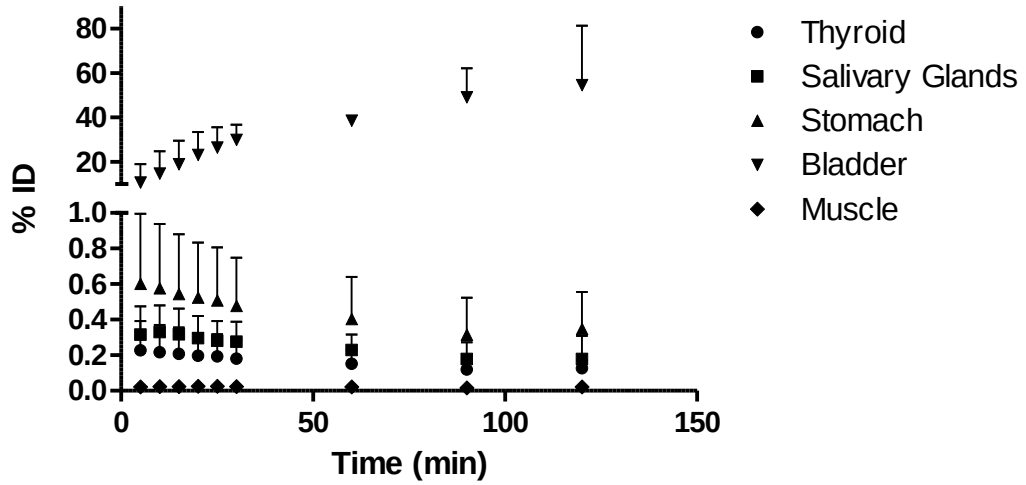

Supplemental Figure 8. Time-activity curve displaying %ID values calculated from PET/CT images for thyroid, salivary glands, stomach, bladder, and muscle over a 2 h time period in BALB/c mice with $NaClO_4$ inhibition (n = 3).

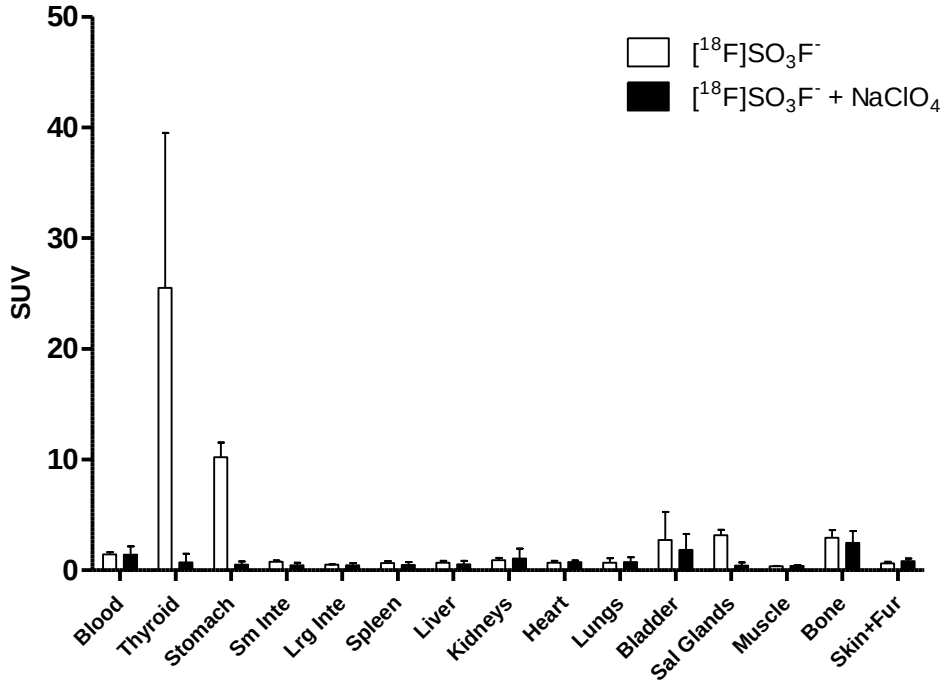

Supplemental Figure 9. *Ex vivo* biodistribution data for $^{18}F\text{-}SO_3F^-$ in BALB/c mice 2.25 h post-injection at (n = 3). Uptake is reported as a standardized uptake value (SUV), which was determined as the ratio of radioactivity in each tissue (MBq) per gram of organ tissue (weighed post-mortem) and radioactivity in the whole body (MBq) per gram of whole body weight (excluding tail). Error bars represent 1 SD.

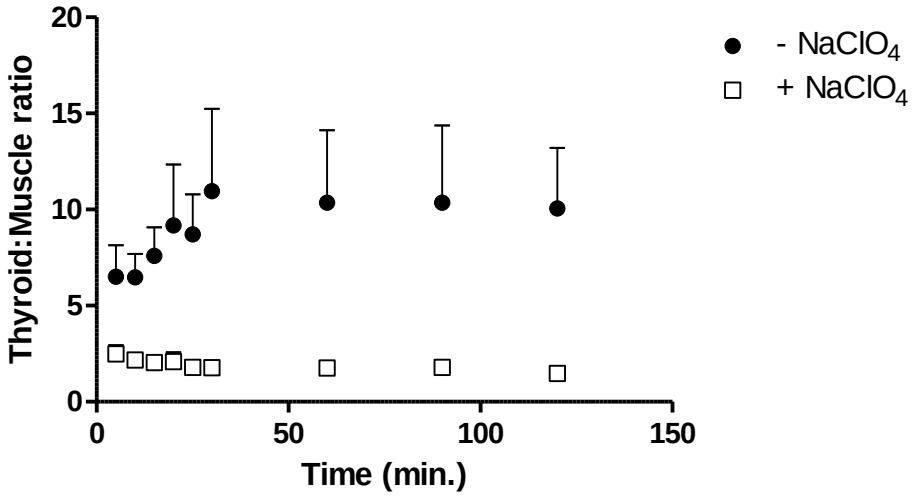

Supplemental Figure 10. Change in ratio of thyroid uptake to muscle uptake (%ID/mL) over time in presence and absence of $NaClO_4$ inhibition (n = 3 per group).

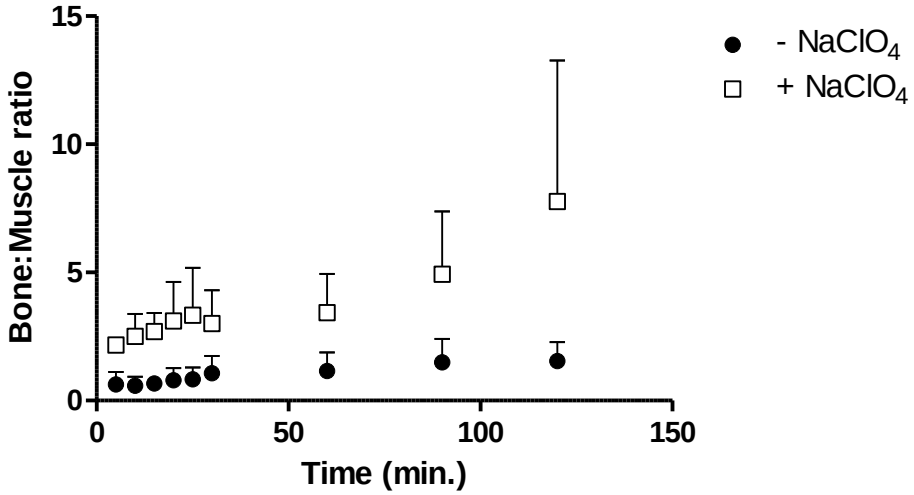

Supplemental Figure 11. Change in ratio of bone uptake to muscle uptake (%ID/mL) over time in presence and absence of $NaClO_4$ inhibition (n = 3 per group).

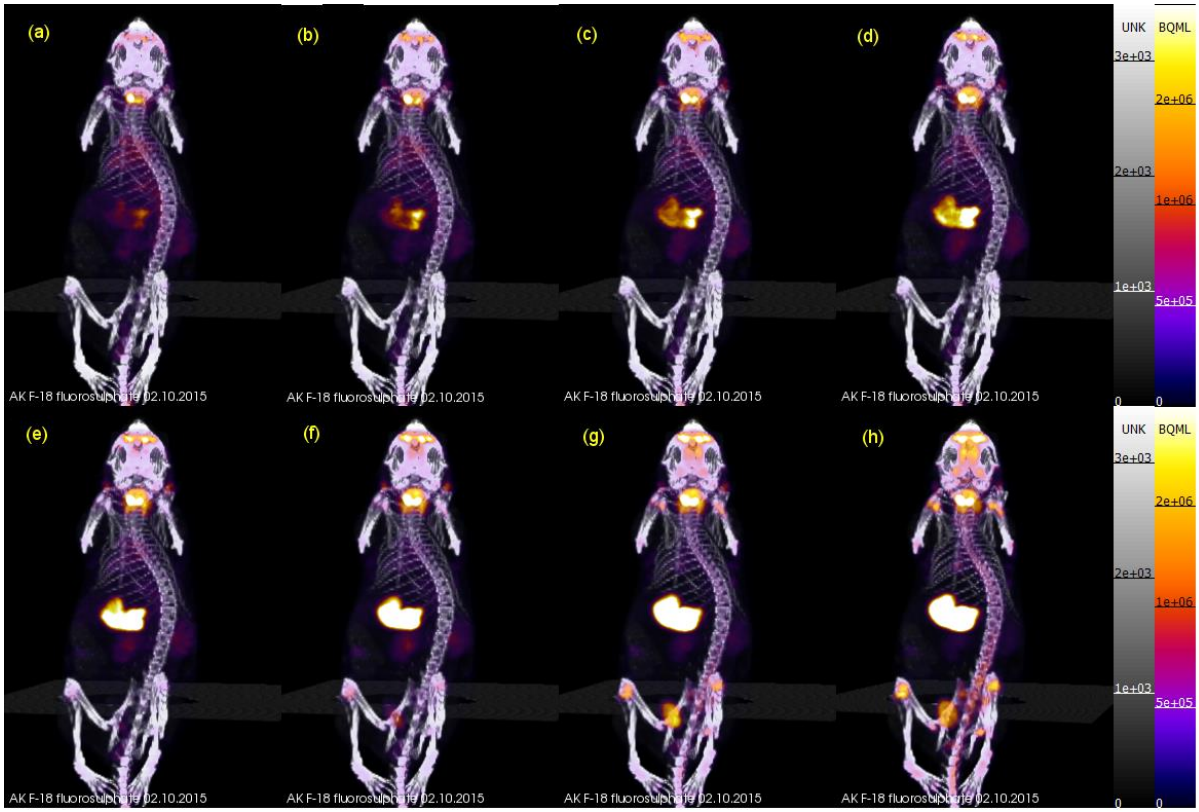

Supplemental Figure 12. PET/CT images of BALB/c mouse following administration of ^{18}F-SO_3F^- at (a) 5 min, (b) 10 min, (c) 15 min, (d) 20 min, (e) 30 min, (f) 60 min, (g) 90 min and (h) 120 min post-injection

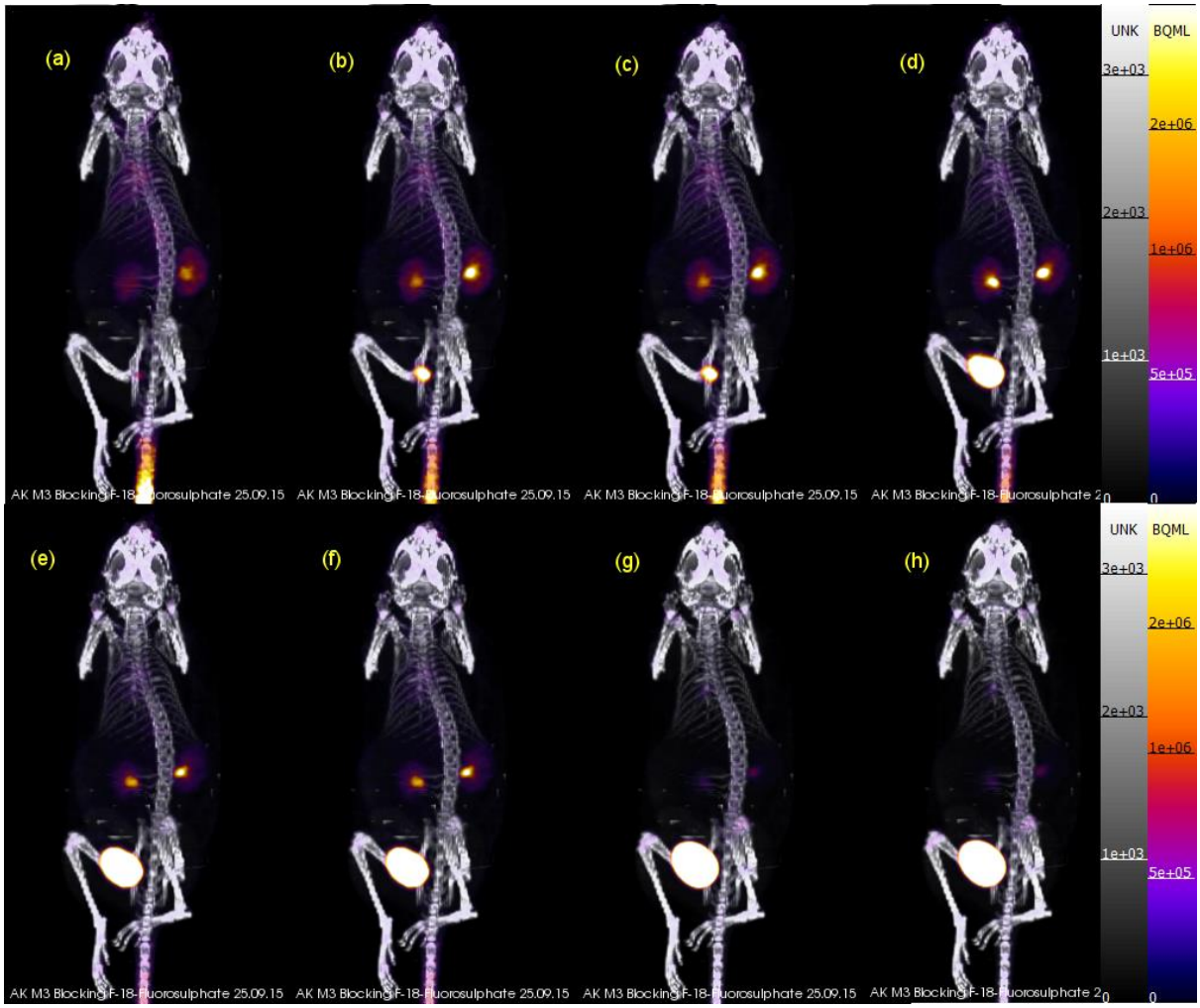

Supplemental Figure 13. PET/CT images of BALB/c mouse following administration of ^{18}F-SO_3F^- and $NaClO_4$ (250 mg/kg) at (a) 5 min, (b) 10 min, (c) 15 min, (d) 20 min, (e) 30 min, (f) 60 min, (g) 90 min and (h) 120 min post-injection.

References

1. Waltz F, Pillette L, Ambroise Y. A nonradioactive iodide uptake assay for sodium iodide symporter function. *Anal Biochem.* 2010;396:91–95.

2. Tonacchera M, Pinchera A, Dimida A, et al. Relative potencies and additivity of perchlorate, thiocyanate, nitrate, and iodide on the inhibition of radioactive iodide uptake by the human sodium iodide symporter. *Thyroid.* 2004;14:1012–1019.

3. Lecat-Guillet N, Ambroise Y. Discovery of aryltrifluoroborates as potent sodium/iodide symporter (NIS) inhibitors. *ChemMedChem.* 2008;3:1207–1209.

4. Weeks AJ, Jauregui-Osoro M, Cleij M, Blower JE, Ballinger JR, Blower PJ. Evaluation of [^{18}F]-tetrafluoroborate as a potential PET imaging agent for the human sodium/iodide symporter in a new colon carcinoma cell line, HCT116, expressing hNIS. *Nucl Med Commun.* 2011;32:98–105.

5. Khoshnevisan A, Jauregui-Osoro M, Shaw K, et al. [^{18}F]tetrafluoroborate as a PET tracer for the sodium/iodide symporter: the importance of specific activity. *EJNMMI Res.* 2016;6:34

6. Jenkins HDB, Roobottom HK, Passmore J, Glasser L. Relationships among ionic lattice energies, molecular (formula unit) volumes, and thermochemical radii. *Inorg Chem.* 1999;38:3609–3620.